Available online at www.sciencedirect.com
SCIENCE DIRECT®
Electrochimica Acta 49 (2004) 4701–4707
ELECTROCHIMICA Acta
www.elsevier.com/locate/electacta

Capacitance and photoelectrochemical studies for the assessment of anodic oxide films on aluminium

J.C.S. Fernandes[a,*], R. Picciochi[a], M. Da Cunha Belo[a], T. Moura e Silva[b], M.G.S. Ferreira[a,c,1], I.T.E. Fonseca[d,1]

[a] *Department of Chemical Engineering, Instituto Superior Técnico, 1049-001 Lisboa, Portugal*
[b] *Instituto Superior de Eng. de Lisboa, Department of Mechanical Engineering, 1950-062 Lisboa, Portugal*
[c] *Department of Ceramics and Glass Engineering, University of Aveiro, 3810-193 Aveiro, Portugal*
[d] *CECUL, Faculty of Sciences, University of Lisbon, 1749-016 Lisboa, Portugal*

Received 5 February 2004; received in revised form 18 May 2004; accepted 19 May 2004

Available online 25 June 2004

Abstract

Photoelectrochemical spectroscopy and capacitance measurements were used in this work to assess the electronic properties of the oxide films formed on 99.5% aluminium and 2024-T3 aluminium alloy by anodising in a sulphuric-boric bath. The morphology of these films was also studied by transmission electron microscopy cross-section observations.

The results obtained indicate that the oxide films formed on aluminium show a n-type semiconductive behaviour, with bandgap energies that are identical for the oxides studied, despite their different characteristics.

It was found out that capacitance measurements may be used as a valuable technique for the assessment of the quality of anodised layers, allowing the distinction between an efficient and an inefficient sealing. Therefore, they may be used to predict the corrosion resistance of these materials.

Keywords: Aluminium; Anodising; Semiconductivity; Capacitance; Photoelectrochemistry

1. Introduction

Corrosion protection of metals and alloys is often achieved by the formation of passive oxide films, which usually exhibit semiconductive properties. The resistance of the metal to corrosive attack has been found to depend upon the solid-state characteristics of the oxide film [1,2]. In this frame, photoelectrochemical spectroscopy and capacitance measurements (Mott–Schottky approach) have been successfully used in the past as in situ techniques for the characterization of passive films formed on different metals [3–5].

Although anhydrous Al_2O_3 has been usually reported in the literature as an insulator, with a bandgap ranging from 8 to 9 eV [6], recent studies of the oxide films formed on aluminium seem to indicate that they show n-type semiconducting properties, with optical transitions ranging between 2.8 and 4.5 eV [7-9]. It should be pointed out that the distinction between a semiconductor and an insulator is however purely arbitrary. In both cases the electronic structure can be described by the band model, but the bandgap of insulators is generally higher than that of semiconductors and the absence of suitable dopants prevents conductivity.

The relationship between the solid-state properties of Al oxide films and its corrosion resistance has been studied through different approaches. McCafferty [7] reported a dependence of the pitting potential on the flatband potential (E_{fb}) and the isoelectric point of the oxide. Similar results were presented by Menezes et al. [8], who found out that E_{fb} increases with the tendency of Al to undergo pitting. On the other hand, Di Quarto and coworkers [9,10] have related the

* Corresponding author. Tel.: +351 218417964; fax: +351 218404589.
E-mail address: joao.salvador@ist.utl.pt (J.C.S. Fernandes).
[1] ISE member.

0013-4686/$ – see front matter © 2004 Elsevier Ltd. All rights reserved.
doi:10.1016/j.electacta.2004.05.025

photoresponse with the different hydration degrees of the surface passive layers.

Anodising of aluminium is a usual process in industry for the enhancement of its anticorrosive properties, and the characteristics of the anodic films formed on aluminium and aluminium alloys have been discussed in a large number of papers [11–15]. The vast majority of these works describe the morphology, chemical composition and structure of the anodic films and are also concerned with kinetics of the film formation processes. However, it is still not possible to ascribe a ''good protective quality'' of the film to a well-known chemical or structural factor.

In the past [13,14], the authors have studied the morphology and anticorrosive properties of anodic films formed by an anodising procedure based on a sulphuric/boric electrolyte, giving special attention to the different oxide structures obtained on pure aluminium and on the aluminium alloy 2024-T3 and to the effect of sealing. Following that work, photoelectrochemical spectroscopy and capacitance techniques were used to assess the electronic properties of anodic oxide films formed by the same process, in order to obtain information on the electronic structure of these films that could allow the development of a schematic model for its band structure, which will be published elsewhere. However, during the experimental part of that work it became evident that these techniques may give valuable information on the characteristics of an anodic film, as different patterns are observed for anodised samples prepared under different conditions. Thus, the present paper is intended to show the usefulness of capacitance measurements as a tool for assessing the quality of anodic oxide films.

2. Experimental

Commercial aluminium (99.5%) and AA 2024-T3 coupons were used.

Before being anodised, the specimens were degreased with acetone, followed by etching in 50 g l^{-1} NaOH solution (2 min, 40 °C) and de-smutting in 50% (v/v) HNO_3 solution (30 s). The sulphuric–boric anodising (SBA) process was carried out during 5, 10, 30 or 60 min at 22 °C, with a constant current of 1.5 A dm^{-2}, in a bath consisting in a mixture of H_2SO_4 (15%) with a solution containing 0.5 M H_3BO_3 and 0.05 M $Na_2B_4O_7{\cdot}10H_2O$, in the proportion 70/30 (v/v). After anodising, some of the specimens were sealed in boiling reagent grade water (Millipore) for 30 min.

Photoelectrochemical measurements were performed, using a 150 W xenon lamp, either at fixed wavelength, varying the applied potential, or at a fixed potential of 0.75 V (SCE). In the later case, the 1200/mm grating monochromator (ORIEL 77200) swept the wavelength between 200 and 700 nm. For the measurement of the photocurrent, the beam was chopped at a frequency of 19 Hz by a 7505 RI chopper synchronised by an EG&G 5210 lock-in amplifier. Because the flux of photons is wavelength dependent, the photocurrent had to be normalised with respect to the incident flux, which was measured by means of a detector (ORIEL 71832-Si), and a current amplifier (ORIEL 70710). This correction of the measured photocurrent yields the quantum efficiency, η_q, of the photoelectrochemical process.

Capacitance versus potential results were obtained by ac impedance measurements at a fixed frequency of 3160 Hz using a sinusoidal potential wave with an amplitude of 10 mV (RMS). Measurements were performed in a potential range of −1.6 to +8 V, at intervals of 0.1 V, using a 273A EG&G potentiostat and a 5210 EG&G lock-in amplifier.

Both photoelectrochemical and capacitance measurements were performed in 0.5 M Na_2SO_4 solution, where the aluminium/aluminium oxide system is considered to be stable.

Sealed and unsealed specimens were observed on a transmission electron microscope (TEM), in order to assess the different structures of the anodic oxides.

3. Results and discussion

3.1. Photoelectrochemical studies

In Fig. 1, the photoelectrochemical response obtained at 200 nm as a function of the applied potential is presented. Both cathodic and anodic photocurrents were observed, at potentials lower and higher than approximately −0.9 V.

The photoelectrochemical response of a semiconductor is dependent on its electronic structure. Taking into account the Gärtner model [16] and introducing some simplifications [17], the quantum efficiency η_q for semiconducting electrodes, defined as the ratio between the photocurrent I_{ph} and the incident photon flux ϕ_o, is given by the following relationship:

$$\eta_q = \frac{I_{ph}}{\Phi_0} = eAw\frac{(h\nu - E_g)^n}{h\nu}$$

where A is a constant, e the elementary charge, w the space charge layer thickness, E_g the bandgap energy and $h\nu$ the

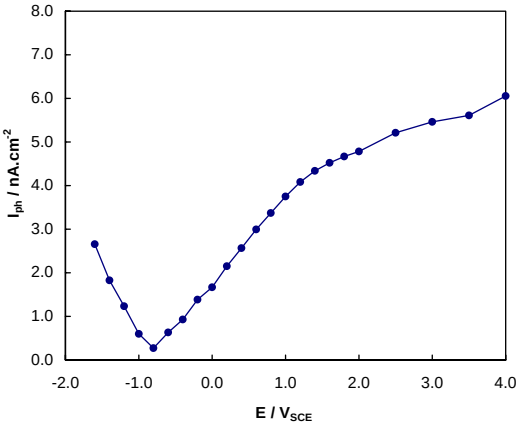

Fig. 1. Photocurrent vs. potential plot obtained in 0.5 M Na_2SO_4 for commercial aluminium (99.5%) as-received.

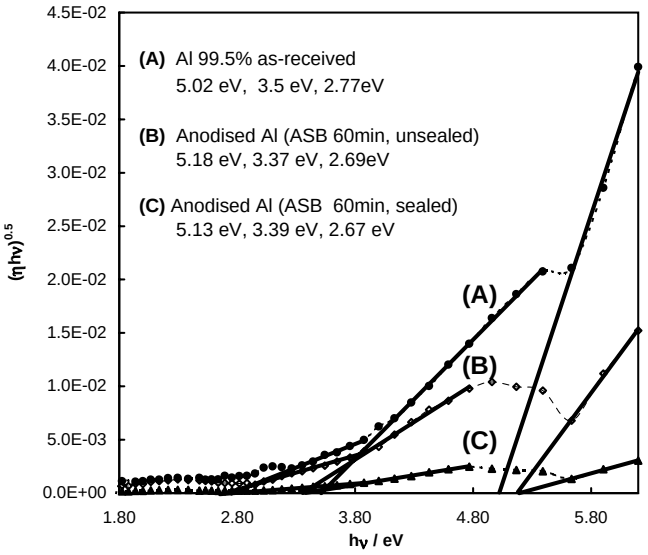

Fig. 2. $(\eta h\nu)^{0.5}$ vs. incident light energy plots, obtained in 0.5 M Na_2SO_4, for commercial aluminium (99.5%): (A) as-received; (B) after 60 min SBA, unsealed; (C) after 60 min SBA, hot water sealed.

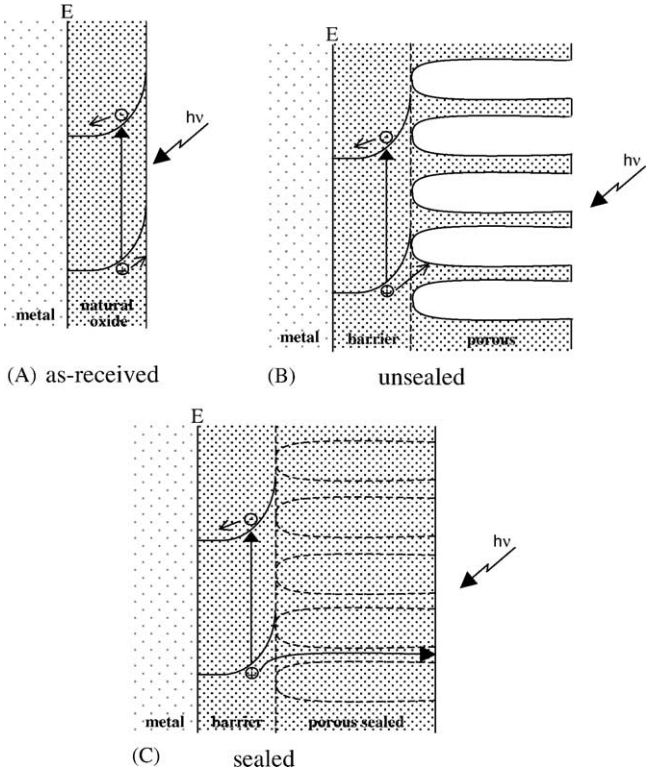

Fig. 3. Schematic band diagrams proposed for aluminium at $E >> E_{fb}$ (A) as-received; (B) after anodising, unsealed; (C) after anodising, hot water sealed.

photon energy. The value of n depends on the type of transition between the valence and conduction band and in this work it was assumed $n = 2$, corresponding to indirect optical transitions. However, other kind of transitions is not ruled out and is being considered for future work.

The results obtained using this approach to the photoelectrochemical spectroscopy measurements performed on commercial aluminium, as-received and after 60 min SBA anodising, unsealed and hot water sealed, are presented in Fig. 2.

Apparently, a semiconductive behaviour of the oxide films obtained in all the three conditions is found, since a photocurrent was measured which at this applied potential is anodic, as it can be observed in Fig. 1. The fact that the applied anodic potential bias is low ($E = 0.75$ V versus SCE) results in a very small thickness of the space charge layer where the holes and electrons are efficiently separated and hence in a small thickness of the layer being sampled, resulting in low photocurrent values.

In each one of the spectra, three different regions may be defined where a linear relationship between $(h\nu\eta_q)^{0.5}$ and $h\nu$ is observed. From the fitting of these regions, it is possible, according to the above equation, to determine values of transition energies, which are identical for the three oxides, despite their different characteristics. In fact, the untreated aluminium of Fig. 2A is only covered by a thin natural oxide film, with a maximum thickness of about 15 nm [18,19], whereas in the two other cases thick oxide films of a few microns were produced during the anodising process. Moreover, it is interesting to note that the major difference between the three spectra is related with the quantum efficiency values. This fact may be interpreted according to the schematic band diagrams depicted in Fig. 3. Upon incidence of the photon beam, a separation of the photogenerated carriers occurs, with electrons moving towards the metal and holes migrating to the oxide/solution interface, where they are consumed. Assuming that the photoactivity is due to the oxide layer adjacent to the metal, then in the case of a specimen only covered by its natural oxide film, an easy transport of holes to the oxide/solution interface is expected. On the contrary, when an unsealed anodic film is present (and considering that the photoactive film is still the one adjacent to the metal) the flow of holes to the oxide/solution interface is hindered. This effect is even stronger when the porous anodic film is sealed. The lower values of quantum efficiency obtained for the sealed material can, therefore, be ascribed to a higher recombination rate of the hole-electron pairs created by the incident photons, as hole transport through a thicker layer is more difficult.

The interpretation of the photocurrent spectra, namely the presence of three distinct extrapolation energies, is very complicated, as transitions from bandgap states (electron traps) into the conduction band, transitions from the valence band to bandgap states (hole traps), transitions from the valence band to the conduction band and transitions from surface states to the conduction band have to be considered. Furthermore, there is an important controversy concerning the interface where photoeffects are controlled [20]: the metal/oxide interface, by means of photoinjection processes (i.e., transitions from the Fermi level of the metal to the conduction band in the oxide film), or the space charge region of the oxide/electrolyte interface, by the creation of

hole–electron pairs. In the present work, photoinjection must be ruled out, since it would result in cathodic photocurrents, whereas the values obtained are anodic.

Concerning the two lower values of energy levels determined for the different samples, they are very similar to those found in the literature [9,10,20], with a slight shift towards lower energies that could be related to different surface preparation [9]. Di Quarto and coworkers [10] also obtained two low energy transitions in the photocurrent spectra, at ca. 3 eV and 3.5–3.7 eV. According to these authors, the two values can be originated by the presence, in the outer part of the internal oxide film, of two hydrated layers with different hydration contents. On the other hand, the higher transition found at ca. 5.15 eV is in the energy range of the various values reported in the literature for the bandgap of anhydrous Al_2O_3 (5.1–8.7 eV, increasing with the cristallinity degree [20,21]). Thus, the photoelectrochemical response of the passive film under irradiation would arise from the contributions coming from three different phases with hydration contents increasing from the inner to the outer layer and, therefore, presenting different optical gaps and photocarriers transport properties.

Another approach may be used to explain the different transitions observed by assuming a distribution of electronic states within the mobility gap of the aluminium oxide films [22].

In order to clarify the above points-of-view and to obtain information on the electronic structure of these anodic oxide films that could allow the development of a schematic model for its band structure, a more fundamental approach is still being followed, which will be published elsewhere.

3.2. Capacitance measurements (Mott–Schottky approach)

It is well established that the capacitance behaviour of a semiconductor–electrolyte interface is similar to that of a semiconductor–metal Schottky junction [23]. Thus, the effect of the applied potential E on capacitance values is described by the Mott–Schottky equation:

$$\frac{1}{C^2} = \frac{2}{\varepsilon\varepsilon_0 q N_d}\left(-E + E_{fb} + \frac{kT}{q}\right)$$

where N_d is the carrier concentration (donor or acceptor), ε the dielectric constant of the semiconductor, ε_0 the vacuum permittivity, q the elementary charge ($-$e for electrons and +e for holes), k the Boltzmann constant, T the temperature and E_{fb} the flatband potential. This equation predicts a linear C^{-2} versus E plot where the point of intersection with the E-axis gives the flatband potential.

In Fig. 4a, it is presented a C^{-2} versus E plot obtained for commercial aluminium, as-received, in 0.5 M Na_2SO_4 solution. As it can be seen, the capacitance values decrease with the applied potential, leading to the development of a straight line with positive slope in the C^{-2} versus E plot. This fact indicates an n-type semiconducting behaviour for the natural Al oxide, in agreement with the literature [7,24] and with the photoelectrochemical results presented above.

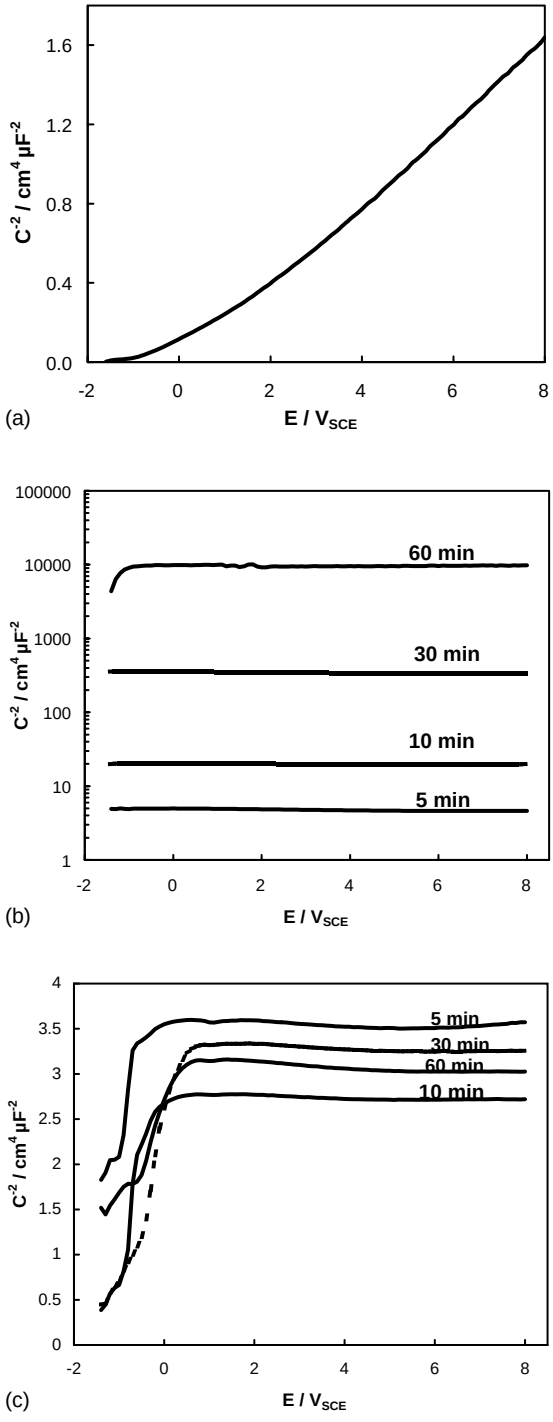

Fig. 4. C^{-2} vs. E plots, obtained in 0.5 M Na_2SO_4 solution, on commercial aluminium (99.5%): (a) as-received; (b) after SBA (5, 10, 30 and 60 min anodising) and hot water sealing; (c) after SBA (5, 10, 30 and 60 min anodising), unsealed.

The influence of film growth during the potential sweep used for the capacitance measurement must not be ignored, as it could account for a decrease in the capacitance values. However, film growth is not the only cause for the changes in

capacitance. In that case, assuming that the growth rate would be proportional to the potential and according to the relationship between the capacitance values and film thickness ($C = \varepsilon\varepsilon_0/d$, where d is the film thickness) the plot of $1/C$ versus E would be linear. On the contrary, the present results depict a linear relationship between C^{-2} and E, which is typical of a semiconductor.

For commercial aluminium samples anodised by the SBA process and hot water sealed (Fig. 4b), the C^{-2} versus E plot presents a quite different shape, as C^{-2} is constant in the entire potential range, indicating a dielectric behaviour of the oxide film. This different behaviour, when compared with the natural aluminium oxide, may be due to the increased thickness of anodic oxide and to its duplex structure. The capacitance measured in this case is the result of a series arrangement of the two capacitances associated with each one of the oxide layers. Considering that the porous layer shows a lower capacitance [12,13,25], then the Mott–Schottky plot only reflects the contribution from this layer. Thus, even if the inner layer presents a semiconductor behaviour, generating a photocurrent, its response in the Mott–Schottky measurements may not be detectable.

Moreover, constant capacitance values obtained in this case are characteristic of the anodic oxide film produced and show a strong dependence on the anodising time. In fact, assuming that the insulating film behaves as a parallel plate capacitor, its capacitance C will depend on the thickness d, in the form $C = \varepsilon\varepsilon_o/d$. As the anodising procedure results in the formation of a duplex anodic film, whose porous layer thickness is proportional to the anodising time, and the subsequent sealing closes efficiently the pores, longer anodising times will then produce a thicker dielectric with lower capacitances and, though, higher values of C^{-2}.

For commercial aluminium samples anodised by the same SBA process but unsealed, the C^{-2} versus E plot (Fig. 4c) reveals a similar dielectric behaviour, but in this case, the constant capacitance values obtained are almost identical, independent of the anodising time and much higher than the ones obtained for sealed anodic oxides. The reason for this behaviour may be found on the duplex structure of the anodic film, which in this case was not sealed. As the presence of pores leads to a short-circuiting of the response of the porous oxide, the capacitance measured is only related to the barrier layer. On the other hand, this barrier oxide reaches its maximum thickness during the first few seconds of anodising, as shown in the voltage versus time plot obtained during the anodic treatment (Fig. 5) where barrier film formation corresponds to the ascending initial line and the porous layer grows at constant voltage [11]. Thus, the maximum thickness of the barrier layer has been obtained for all the samples, regardless the anodising time, so the associated capacitance is expected to be the same, as observed.

The capacitance results obtained in the same solution for the aluminium alloy 2024-T3 anodised by the SBA process with different anodising times and unsealed are presented in

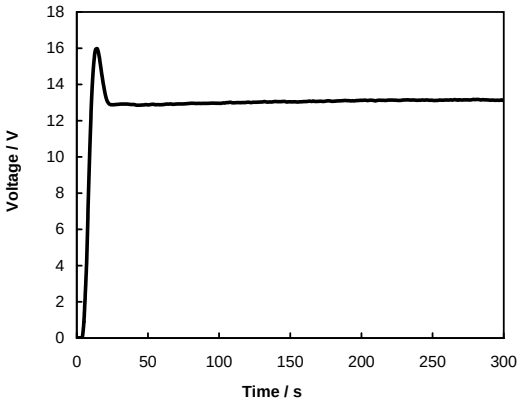

Fig. 5. Voltage vs. time plot obtained during SBA anodising of commercial aluminium.

Fig. 6a. With the exception of an initial step, up to approximately −200 mV (versus SCE), which could be attributed to the presence of active copper-rich precipitates that become oxidized for higher potentials, the oxide behaves as an insulator, showing horizontal C^{-2} versus E lines. Similarly to commercial aluminium, no influence of the anodising time is detected, which may be explained by the same arguments, i.e., for a unsealed duplex anodic oxide the capacitance response measured is due to the barrier layer, whose thickness is independent of the anodising time.

For the Al 2024-T3 samples anodised by the SBA process and hot water sealed, the C^{-2} versus E plots (Fig. 6b) are quite similar to those obtained for the unsealed material and, in particular, no dependence on the anodising time is observed. The reason for this different behaviour of the 2024-T3, compared with the commercial aluminium, may be found on the anodic oxide structures observed on the TEM micrographs of the two materials (Fig. 7). In fact, the pores formed during anodising of 99.5% aluminium, which are linear, continuous and perpendicular to the surface, may be easier to seal than the tortuous pores found for the 2024 alloy. In the latter case, the sealing process is less effective and the formation of the hydrated layer is restricted to a superficial zone of the porous oxide, which can be easily penetrated by the solution during exposure to the test solution. This different sealing behaviour between 99.5% aluminium and the 2024 alloy is also detected for other anodising baths, such as the sulphuric acid or the chromic acid baths [13,14], as the oxide structure is nearly the same for each one of them.

The assessment of the anticorrosive properties achieved by the above-mentioned anodic treatments, compared with more traditional anodising procedures such as sulphuric acid anodising and chromic acid anodising, has been recently published by the authors. In that papers [13,14] it is concluded that the different structure of the anodic oxides formed in the 2024-T3 alloy, regardless the anodising procedure used, may be explained as the effect of oxygen evolution occurring preferentially on the copper-rich precipitates that are present in this alloy. Moreover, this

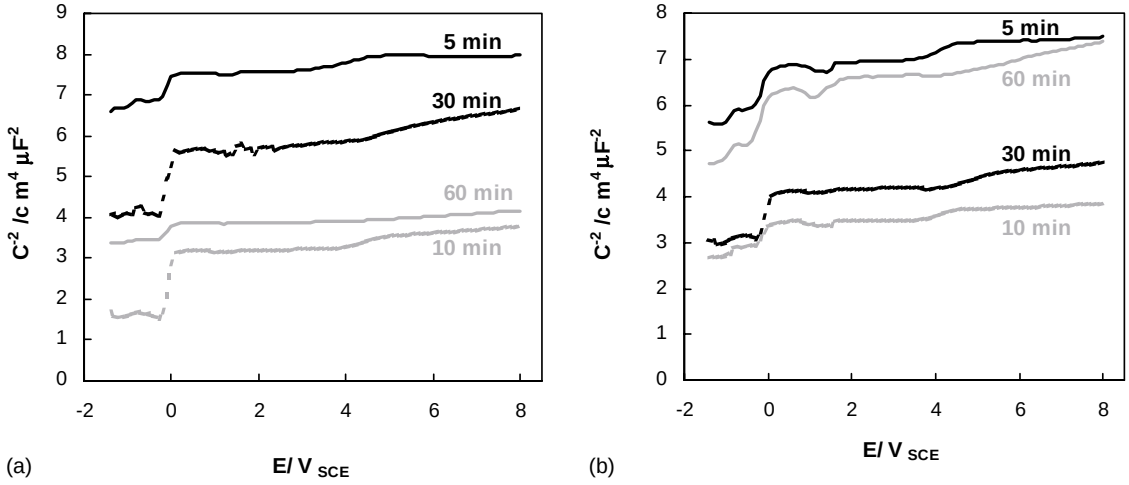

Fig. 6. C^{-2} vs. E plots, obtained in 0.5 M Na_2SO_4 solution, for aluminium alloy 2024-T3 after SBA (5, 10, 30 and 60 min anodising): (a) unsealed; (b) hot water sealed.

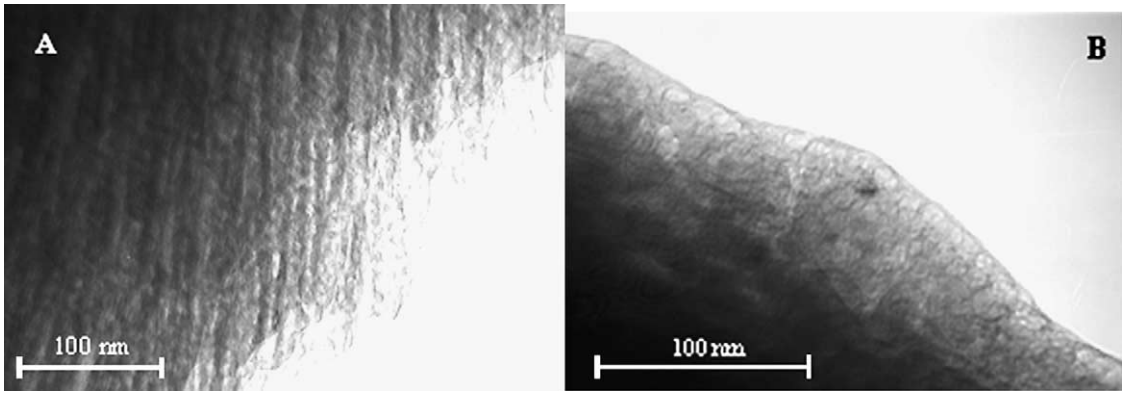

Fig. 7. TEM cross-sections of samples anodised in a sulphuric–boric bath and not sealed: (A) 99.5% aluminium; (B) AA 2024-T3.

structure is responsible for the above-mentioned difficulty in achieving a good sealing, which accounts for the inferior corrosion resistance of anodised 2024-T3.

In this perspective, capacitance measurements may be regarded as a useful technique for the assessment of the quality of anodised layers. As shown above, this method allows the distinction between an efficient and an inefficient sealing and therefore it may be used to predict the corrosion resistance of these materials.

4. Conclusions

The photoelectrochemical spectroscopy measurements indicate that the oxide films formed on aluminium show a semiconductive behaviour. Three different optical transitions were determined, which are identical for the oxides studied, despite their different characteristics. Moreover, from the photoelectrochemical and capacitance measurements performed on commercial aluminium it is possible to ascribe an n-type semiconductive behaviour, in accordance to the literature.

In face of the complexity of a more fundamental interpretation for the results obtained, that is being carried out at the moment, it was found out that capacitance measurements may be used as a valuable technique for the assessment of the quality of anodised layers. For non-anodised aluminium the semiconductive behaviour of its natural oxide was clearly revealed, whereas the anodised materials have shown a dielectric response in the C^{-2} versus E plots. Moreover, this response is very sensitive to the changes of the oxide film occurred during the sealing procedure, revealing that this process is ineffective in the case of the 2024-T3 alloy. The reason for this fact is related to the tortuous structure of the porous oxide formed on this material, as observed by transmission electron microscopy.

Thus, it may be concluded that capacitance measurements allow the distinction between an efficient and an inefficient sealing and, therefore, may be used to predict the corrosion resistance of these materials.

Acknowledgments

The authors acknowledge the Portuguese Science and Technology Foundation (FCT) for the financial support under the Operational Programme of Science, Technology and Innovation (POCTI).

References

[1] N. Sato, Corrosion 45 (1989) 354.
[2] Z. Szklarska-Smialowska, Corros. Sci. 44 (2002) 1143.
[3] A.M.P. Simões, M.G.S. Ferreira, B. Rondot, M. da Cunha Belo, J. Electrochem. Soc. 137 (1990) 82.
[4] U. Stimming, Electrochim. Acta 31 (1986) 415.
[5] P.C. Searson, R.M. Latanision, U. Stimming, J. Electrochem. Soc. 135 (1988) 1358.
[6] W.H. Strehlow, E.L. Cook, J. Phys. Chem. Ref. Data 2 (1973) 163.
[7] E. McCafferty, Corros. Sci. 54 (2003) 301.
[8] S. Menezes, R. Haak, G. Hagen, M. Kendig, J. Electrochem. Soc. 136 (1989) 1884.
[9] G. Tuccio, S. Piazza, C. Sunseri, F. Di Quarto, J. Electrochem. Soc. 146 (1999) 493.
[10] S. Piazza, C. Sunseri, F. Di Quarto, Corrosion 58 (2002) 436.
[11] S. Tajima, in: M.G. Fontana, R.W. Staehle (Eds.), Advances in Corrosion Science and Technology, vol. 1, Plenum Press, New York, 1970 (Chapter 4).
[12] T.P. Hoar, G.C. Wood, Electrochim. Acta 7 (1962) 333.
[13] L. Domingues, J.C.S. Fernandes, M. Da Cunha Belo, M.G.S. Ferreira, L. Guerra-Rosa, Corros. Sci. 45 (2003) 149.
[14] L. Domingues, J.C.S. Fernandes, M.G.S. Ferreira, in: Proceedings of the 15th ICC, Granada, Spain, 2002 (Paper 444).
[15] J.J. Suay, E. Gimenez, T. Rodriguez, K. Habbib, J.J. Saura, Corros. Sci. 45 (2003) 611.
[16] W.W. Gärtner, Phys. Rev. 116 (1959) 84.
[17] Y. Pleskov, Y. Gurevich, in: B.E. Conway, C.R. White, J.O'M. Bockris (Eds.), Modern Aspects of Electrochemistry, vol. 16, Plenum Press, New York, 1985.
[18] J.E. Graedel, J. Electrochem. Soc. 136 (1989) 204C.
[19] R.S. Alwitt, J. Electrochem. Soc. 121 (1974) 1322.
[20] F. Di Quarto, C. Gentile, S. Piazza, C. Sunseri, J. Electrochem. Soc. 138 (1991) 1856.
[21] J.P. Sukamto, C.S. McMillan, W. Smyrl, Electrochem. Acta 39 (1993) 15.
[22] F. Di Quarto, S. Piazza, C. Sunseri, in: S.G., Pandalai, (Ed.), Current Topics in Electrochemistry, vol. 3, Trivandrum, 1994. p. 357.
[23] Y. Pleskov, Y. Gurevich, in: P.N. Bartlett (Ed.), Semiconductor Photoelectrochemistry, Consultants Bureau, New York, 1986.
[24] J.O'M. Bockris, Y. Kang, J. Solid State Electrochem. 1 (1997) 17.
[25] F. Mansfeld, M.W. Kendig, J. Electrochem. Soc. 135 (1988) 828.